Characterisation of Electrical Loading Experienced by a Nacelle Power Converter

C.J. Smith[a], G.N. Wadge[a], C.J. Crabtree[a], P.C. Matthews[a]

[a]Energy Group, School of Engineering and Computing Sciences, Durham University

I.   Abstract

The reliability of fully rated converters (FRC) in permanent magnet synchronous generator (PMSG) wind turbines is critical. A drive train model has been constructed to simulate the current throughput of the power modules in the FRC in response to a variety of isolated wind speed conditions and simulated wind speed profiles to explore potentially damaging operating conditions.

The drive train model is based on a 2MW, PMSG, direct-drive, FRC wind turbine. The mechanical drive train is modelled as a 2-mass model. The machine-side converter (MSC) was parameterised using a Semikron converter. The turbine was controlled via maximum power point tracking (MPPT) and active pitch control.

The results revealed that the turbine inertia and control decoupled the wind and current profiles. Pitch control overshoot leads to long term current variation even when operating at above rated wind speed. Therefore the wind speed cannot be used to directly derive the MSC currents. Instead the detailed wind turbine drive train model presented is required for MSC current simulation.

With this current response, detailed simulation and analysis of the MSC thermal loading is possible. The turbine can now be emulated in an experimental rig using an AC power supply to provide realistic operating conditions.

Keywords – Power Converter Reliability, Power Module Current, Drive Train Model, Simulation

II.   Introduction

To meet EU renewable energy targets for 2020 and beyond, the Levelised Cost of Energy (LCoE) of offshore wind needs to be reduced to below £100/MWh [1]. Operation and maintenance (O&M) costs account for around 30% of the LCoE [2] and therefore research has focused on understanding the reliability of components and their impact on the LCoE.

In the past turbine topologies have been modified in response to poor reliability. A number of onshore turbine failure datasets have been examined [3] to find the components causing wind turbine failure. It is broadly accepted that generator and mechanical subsystem failures have led to the longest downtimes. In response turbine manufacturers have introduced direct-drive topologies or simplified the gearbox to improve reliability.

Wind turbine drive trains have also introduced more power electronic devices to allow for variable speed operation for improved energy capture. However these devices have a large number of sensitive components which has led to a concern that these devices will lead to poorer reliability.

[4] examined a large dataset for offshore wind turbines with varying turbine technology to determine the main causes of failure and concluded that the power converter had a typical failure rate of ~0.2 failures/turbine/year (f/t/y) over the turbine population, much lower than components such as the pitch system (~1.1 f/t/y). However this study did not distinguish between turbine technology and the extent power converters are used.

A more focused study on turbine type [5] found that the failure rate of fully-rated converters (FRC) in permanent magnet synchronous generator (PMSG) turbines was 0.593 f/t/y compared to the 0.106 f/t/y for doubly fed induction generator (DFIG) turbines. This FRC failure rate is three times higher than the rest of the turbine population. Of these failures, power modules are the failure mode for nearly all major converter repairs. FRC reliability is critical for PMSG turbines, with power module failure the most critical failure mode.

The reduction in reliability when moving to offshore has been noted as a key concern. This is due to the increased repair times and cost to repair over onshore turbines [6]. Onshore, the converter reliability has been largely ignored as it is relatively easy to repair or replace compared to many of the mechanical components. However, with reduced accessibility, a converter failure offshore is much more critical to the overall performance of the turbine [7]. A small failure in the converter in bad weather could lead to a logistical delay of up to half a year in extreme circumstances [8]. This issue of reduced reliability offshore leads to loss in power generation and a loss of revenue [9], increasing the LCoE.

With power converters becoming increasingly important for turbine reliability, researchers have attempted to predict converter lifetime. Typically this has been carried out using cycles-to-failure against insulated gate bipolar transistor (IGBT) junction temperature swing (ΔT_j) manufacturing data [10]. ΔT_j is calculated by converting power throughput of converters into T_j of IGBT chips using thermal impedance networks. With this T_j data, cycles-to-failure data is used to compute end-of-life.

However, whilst power module failure modes are well understood, manufacturing cycle data is often produced at fixed frequency and magnitude ΔT_j [5]. This is not representative of how a converter is operated in the turbine [10]. Therefore harmful operating conditions may have their impact on reliability omitted.

To address this, an experimental rig is being designed which will apply the power converter under turbine operating conditions. The experiments will focus on extreme operating conditions. Understanding these harmful operating conditions may highlight turbine operations that should be avoided to improve reliability, and provide information on the failure characteristics of power converters for improved maintenance strategies. The rig will also provide opportunities for condition monitoring research.

Prior to this experimental work the potentially harmful operating conditions need to be characterised. This paper outlines a computer simulation of a turbine drive train that is used to meet the following objectives:

- To provide a wind turbine drive train model for characterisation of electrical signals that are experienced by the MSC at different operating points on the power curve.
- To provide data for parameterisation of an experimental rig to test the reliability of MSC under various operating regimes.
- To simulate the electrical signals produced by the generator so an AC power supply can be used in the experimental rig.

The paper is organised as follows. Section III outlines the details of the drive train model constructed, Section IV details the drive train and converter response to various isolated and turbulent wind conditions, and Section V concludes the paper.

III.   Drive Train Modelling

The drive train model needs to be relevant to the modern wind turbine industry. As discussed in Section II, the FRC of the PMSG is proving to be reliability critical and therefore is chosen for study. The state-of-the-art offshore wind turbines being constructed are now reaching 5-6 MW. However, there is not enough

data freely available to be able to simulate this size in appropriate detail. Therefore a 2MW PMSG-FRC drive train was modelled.

The drive train model can be split into 7 sub-systems; rotor power extraction, drive train dynamics, generator, machine-side converter (MSC), DC link, turbine control and simulation details. This section details the key features of the model.

a.   Rotor Power Extraction

First the turbine power extracted by the rotor (P_t) is calculated (1) [11].

$$P_t = 0.5 C_p \rho \pi r^2 u^3 \tag{1}$$

Where C_p is the coefficient of performance, ρ is air density (kg/m^3), r is the rotor radius (m), and u is the wind speed (m/s).

C_p depends on the tip-speed ratio (λ) of the turbine and the blade pitch angle (β). The C_p, λ and β relationship is turbine specific but it is typical to use a numerical approximation (2, 3).

$$C_p = A_t \left(\frac{B_t}{\lambda_i} - C_t \beta - D_t \beta^{E_t} - F_t \right) e^{\frac{-G_t}{\lambda_i}} \tag{2}$$

$$\frac{1}{\lambda_i} = \frac{1}{\lambda + H_t \beta} - \frac{K_t}{\beta^3 + 1} \tag{3}$$

Where A_t - F_t, K_t are turbine specific constants.

The C_p has been plotted for an example turbine in Figure 1. The parameters are available in Table A in Appendix A.
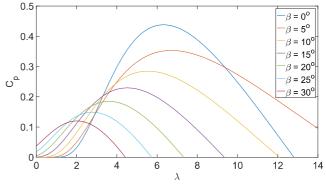

Figure 1: Example C_p-λ curves for turbine rotor with varying β.

λ is the ratio between turbine rotational speed (ω_t) and u and is calculated using (4).

$$\lambda = \frac{\omega_t r}{u} \tag{4}$$

The resultant turbine torque (T_t) is calculated using (5).

$$T_t = \frac{P_t}{\omega_t} \qquad (5)$$

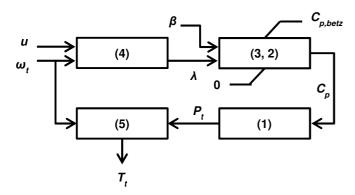Figure 1 summarises the rotor power extraction model.

Figure 1: Summary of rotor power extraction model.

b. Drive Train Dynamics

The T_t extracted from the wind is applied to the drive shaft. As a direct drive turbine was modelled the drive shaft is connected directly to the generator without a gearbox. The drive train can be modelled as a mechanical mass-spring-damper system which dynamically impacts the resulting mechanical torque (T_m) applied to the generator.

Ideally the higher the order of the mechanical system (number of masses and connections), the more accurately the dynamics will be modelled. However, the higher order the modelling, the more computationally expensive the calculations become. Therefore a compromise must be made. In general, drive train models for direct-drive PMSG turbines come in either lumped-mass or 2-mass models. A 3-mass model would be preferred as all fundamental torque oscillations that may interact with the electrical transients can be modelled [12] but no data was found and therefore a 2-mass model was used, as represented in Figure 3.
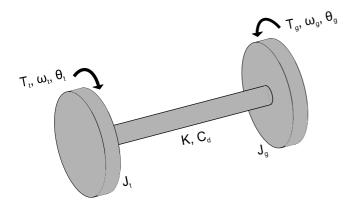

Figure 3: 2-mass model of wind turbine drive train.

J_t, J_g are the moments of inertia of the turbine and generator respectively (kgm^2), ω_g is the rotational speed of the generator (rad/s), Θ_t, Θ_g are the rotational displacements of the turbine and generator respectively (rad), C_d is the shaft damping coefficient (Nms/rad), K is the shaft stiffness (Nm/rad) and T_g is the electromagnetic torque (Nm).

The 2-mass model is described by the following matrix of equations of motion (1.7) [13].

$$\begin{bmatrix} J_t & 0 \\ 0 & J_g \end{bmatrix} \begin{Bmatrix} \alpha_t \\ \alpha_g \end{Bmatrix} + \begin{bmatrix} C_d & -C_d \\ -C_d & C_d \end{bmatrix} \begin{Bmatrix} \omega_t \\ \omega_g \end{Bmatrix} \\ + \begin{bmatrix} K & -K \\ K & -K \end{bmatrix} \begin{Bmatrix} \theta_t \\ \theta_g \end{Bmatrix} = \begin{Bmatrix} T_t \\ T_g \end{Bmatrix} \qquad (6)$$

Where α_t, α_g are the rotational accelerations of the turbine and generator respectively (rad/s^2). This matrix can be expanded to provide a number of equations of motion to be solved numerically (7-11).

$$T'_m = (\omega_t - \omega_g)C_d + (\theta_t - \theta_g)K \qquad (7)$$

$$\alpha_t = \frac{T_t - T'_m}{J_t} \qquad (8)$$

$$\alpha_g = \frac{T'_m - T_g}{J_g} \qquad (9)$$

$$\omega = \int \alpha(t)dt \qquad (10)$$

$$\theta = \int \omega(t)dt \qquad (11)$$

Where T'_m is the resultant torque from the shaft damping and shaft stiffness (Nm).

As the drive train model was solved discretely, the integrations were performed discretely. Figure 4 details the block diagram of the drive train dynamics.
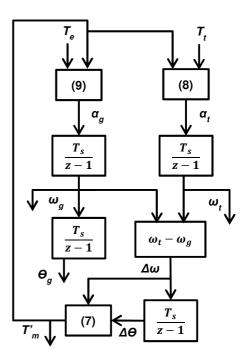

Figure 4: Block diagram of drive train dynamics. T_s is the sample time (s).

c. Generator

The generator used was a non-salient PMSG and was modelled as a 2nd order generator in the *dq0* reference frame [12]. The mechanical component was modelled with the torque swing equation to simulate the acceleration due to difference between mechanical and electrical torque (9).

The generator used for the simulation was Simulink's inbuilt *SimPowerSystems* 'permanent magnet synchronous machine (PMSM)'. The generator parameters can be found in Appendix A.

d. MSC

In a typical wind turbine the converter is comprised of a back-to-back rectifier/inverter. The rectifier acts as the MSC and the inverter acts as the grid-side converter (GSC). The role of the MSC and GSC differs depending on control strategy but the MSC typically controls the speed of the wind turbine for optimum power production whilst the GSC maintains the DC link voltage and controls power extraction to the grid.

Due to turbine speed variation the MSC experiences a more varied operating profile compared to the fixed frequency GSC. The MSC is consequently of greater interest for reliability analysis. Therefore, only the MSC is modelled fully and the GSC is replaced with a constant voltage source to maintain the DC link (Section III.e).

The MSC was modelled as a 2-level IGBT-diode pair active rectifier. Simulink's inbuilt *SimPowerSystems* *'Universal Bridge'* was used and the *'Power Electronic Device'* was set to *'IGBT/ Diodes'*.

The MSC parameters were based on the power modules found in the SEMIKRON SKSB1090GD69/11-MAPB stacks [14]. These stacks have SKiiP1513GB172-3DWV3 half-bridge modules and their data can be found in [15]. The parameters used are detailed in Appendix A.

The current across the devices is taken from the *'Universal Bridge'* module. This current output is split across diode and IGBT and can be determined by the sign convention outlined in [16]. This current must also be halved to determine the current throughput of each power module as 2 parallel stacks are required to provide the power rating for the turbine [17]. Figure 5 outlines the conversion from converter output to device currents. I_{sw2} is the current on one switch from the Simulink model. The positive values of I_{sw2} give the current on the IGBT (I_{IGBT2}) and the negative values give the diode current (I_{Diode2}). These are then halved to give the current in each stack.
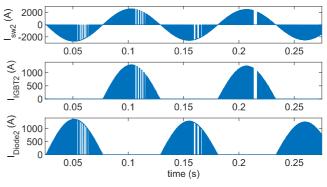

Figure 5: Current output from converter.

To summarise, the MSC of the drive train is modelled as a 2-level IGBT rectifier using Simulink's *'Universal Bridge'* module. The MSC is based on 2 parallel SEMIKRON RE stacks with the model parameters taken from the SKiiP1513GB172-3DWV3 half-bridge.

e. DC Link

As discussed in Section III.d the GSC has been replaced with a fixed voltage supply. Typically for a low voltage PSMG (~690V) the DC link voltage (V_{dc}) is maintained at anywhere between 1000-1300V [12, 18]. Based on the RE stack detailed in Section III.d and the PWM strategy chosen in Section III.f, the DC-link was set to 1150V_{dc} (±575V_{dc}).

f. Turbine Control

Power extraction is controlled in 2 ways; maximum power point tracking (MPPT) for below rated speed, and active pitch control for above rated speed.

MPPT

MPPT is achieved by maintaining C_p at its maximum ($C_{p,max}$) via the an optimum λ (λ_{opt}) (peak in Figure 1) when below rated wind speed. The ω_t must be controlled to maintain this λ_{opt} (12).

$$\omega_{t,opt(u)} = \frac{u\lambda_{opt}}{r} \tag{12}$$

Where $\omega_{t,opt(u)}$ is the optimum turbine rotational speed at a given wind speed (rad/s).

$\omega_{t,opt(u)}$ is achieved using torque control. By varying the T_g, the turbine can accelerate or decelerate (9). To calculate the torque required at a given wind speed ($T_{ref(u)}$), the equation for turbine power (1) and torque (5) can be used to determine a relationship between $\omega_{t,opt(u)}$ and $T_{ref(u)}$ (13-15).

$$P_{t,max} = 0.5C_{p,max}\rho\pi r^2 \left(\frac{r}{\lambda_{opt}}\right)^3 \omega_{t,opt(u)}{}^3 \tag{13}$$

$$K_{MPPT} = 0.5C_{p,max}\rho\pi r^2 \left(\frac{r}{\lambda_{opt}}\right)^3 \tag{14}$$

$$T_{ref(u)} = K_{MPPT}\omega_{t,opt(u)}^2 \qquad (15)$$

Where K_{MPPT} is a turbine specific constant (kgm^2).

As u is not measured in this control strategy, $\omega_{t,opt}$ is unknown at any given point. Instead T_{ref} is calculated using ω_t (16). If $\omega_t \neq \omega_{t,opt}$ then ω_t will continue to change, changing T_{ref} until steady state is reached.

$$T_{ref} = K_{MPPT}\omega_t^2 \qquad (16)$$

This T_{ref} is achieved by varying the current demanded of the generator. For this control the d,q currents ($I_{d,q}$) are used in a $dq0$ control strategy (17, 18), with the $I_{d,q}$ calculated from the stator currents (I_{abc}) via a Park transform.

$$I_{d,ref} = 0 \qquad (17)$$

$$I_{q,ref} = \frac{2p}{3\varphi}T_{ref} \qquad (18)$$

Where $I_{d,qref}$ are the reference d,q currents (A), p is the number of generator poles, and φ is the permanent magnet flux linkage (Vs).

$I_{d,ref}$ is maintained at zero as it relates to magnetisation which is not required for a PMSG machine. Holding the magnetisation current at zero also minimises resistive losses [19].

These currents are achieved by applying a controlled voltage on the generator terminals using the MSC. Again the voltages are processed in the d,q reference frame ($V_{d,q}$). $V_{d,q}$ are determined by using independent Proportional-Integral (PI) controllers that use the error between $I_{d,q}$ and $I_{d,q,ref}$ to produce $V_{d,q}$ errors. These errors are added to the known generator voltages (impedance and armature voltages) to produce the required terminal voltages for the generator ($V_{d,q,ref}$) [12]. $V_{d,q,ref}$ is converted into the abc reference frame ($V_{abc,ref}$) via an inverse Park transform for use by the converter pulse width modulation strategy (PWM). Figure 6 details the $dq0$-control of the MSC.

r_s is the PMSG stator phase resistance (Ω), $L_{d,q}$ are the

PMSG d,q armature inductances (H), and ω_e is the magnetic field rotational speed (rad/s) which calculated using (19).

$$\omega_e = \frac{p}{2}\omega_g \qquad (19)$$

Where $p/2$ is the number of pole pairs in the generator.

The PWM converts the modulated $V_{abc,ref}$ (between -1 and 1) (V_m) into a switching pattern for the IGBTs in order to produce the 3-phase converter output voltage ($V_{c,abc}$). In this case a sine-wave PWM (SPWM) strategy was chosen and implemented using the '*PWM Generator (2-level)*' Simulink block. The carrier mode of operation was set to '*synchronised*' to ensure the carrier frequency remained synchronised to reference signal. The carrier/reference ratio ($R_{c/r}$) can be found in Appendix A.

As the SPWM was used, V_m was calculated using (20).

$$V_m = \frac{2}{V_{dc}} V_{abc,ref} \qquad (20)$$

To summarise, MPPT was achieved by using torque control via $dq0$ vector control of the MSC. SPWM was used to convert the reference voltage signals into switching signals for the IGBTs.

Pitch Control

Pitch control limits power extraction by pitching the blades away from the optimum angle, reducing the turbine's C_p (Figure 1). This pitching occurs above the rated wind speed.

There are a number of control methods available for pitch control [20]. For this work the difference in ω_t and rated ω_t ($\omega_{t,rat}$) was used with a PI-controller to produce a β error (β_{err}) (Figure 7.a). In reality the β-ω_t relationship is not linear but the approximation was found to be adequate for turbine control.

β_{err} is added to the current β to produce a reference β (β_{ref}) and applied to the pitch actuator (Figure 7.b). The pitch actuator is modelled as a 1st order dynamic
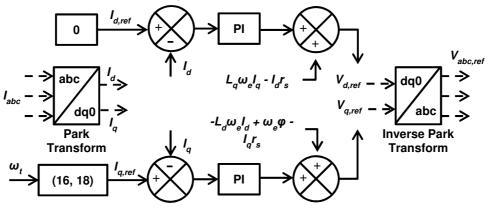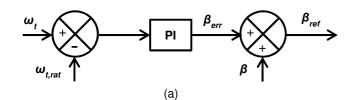

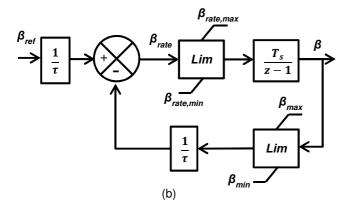Figure 6: Schematic of machine-side controller.

Figure 7: (a) Pitch controller and (b) pitch actuator block diagrams. τ is the actuator time constant (s).

system as found in [21] with limits on β and the rate of change of β (β_{rate}). These values can be found in Appendix A.

g. Simulation Configuration

The Simulink simulation is discretized using the Tustin and Backward Euler method with a T_s of $5\text{x}10^{-6}$s. As the simulation was discretized purely resistive snubbers were needed to simulate having no snubbers in the 'Universal Bridge' [22]. To do this, the default snubber parameters in the 'Universal Bridge' were used (Appendix A).

To tune the PI controllers a simpler model of the drive train was constructed. The PMSG was modelled as found in [23] and the MSC was omitted. Simulink's 'Tune' graphical user interface in the PI controllers was used to tune the controllers before the PI parameters were applied to the more complex model. These parameters can be found in Appendix A.

h. Drive Train Model Summary

The drive train model consists of the following key features:

- Modelled as a direct-drive 2MW wind turbine.
- Mechanical drive train modelled as a 2-mass model.
- 2nd order non-salient PMSG modelled in the *dq0* reference frame
- FRC with MSC based on SEMIKRON RE stacks.
- GSC modelled as an ideal DC link.
- Turbine controlled using ω_t as the reference signal.
- MPPT achieved using *dq0* vector control.
- MSC switching achieved using SPWM.
- Power limited above rated wind speed using active pitch control and a 1st order dynamic system actuator model.

IV. Results

This section outlines the drive train model response to a reduction in wind speed in the MPPT operating region (Section IV.a), a ramp up in wind speed from MPPT to rated operation (Section IV.b), and a
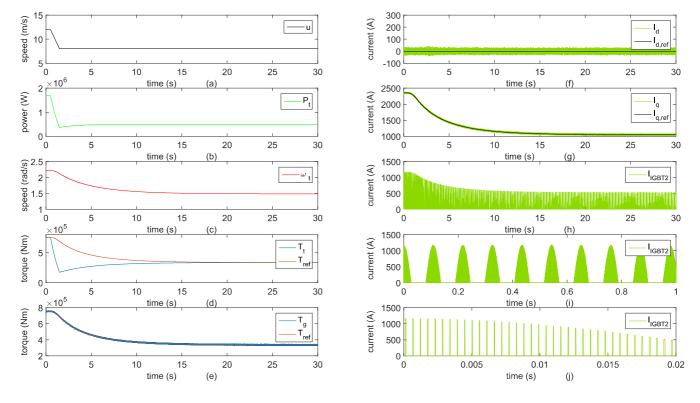

Figure 8: Turbine Response to reduction in wind speed: (a) wind speed, (b) turbine power, (c) turbine speed, (d) turbine torque, (e) generator torque, (f, g) generator *d,q* current and (h-j) IGBT current.

turbulent wind speed input (Section IV.c).

a. Wind Speed Reduction in MPPT Operating Region

Figure 8 details the turbine response to a reduction in wind speed from 12m/s to 8m/s in the MPPT operating region. Figure 8.d-g shows that the turbine model successfully responds to the variation in wind speed.

This turbine response is dictated by the change in ω_t (Figure 8.c). As the ω_t is influenced by the turbine inertia the turbine response is much smoother than the sudden change in wind speed (ω_t reaches steady state ~22s after the wind speed event has finished).

The I_q response follows the ω_t response very closely with negligible overshoot (Figure 8.g) and I_d remains at approximately 0A (Figure 8.f). The negligible overshoot on the I_q response can be attributed to the slow turbine response leading to small I_q errors over time. Furthermore, by following the ω_t response, the current throughput is smoothed and maintains a higher current than if the current was directly derived from the wind speed. Therefore, these results indicate that the drive train dynamics cannot be neglected when determining the current throughput of the converter.

There is noise on both I_d and I_q signals (Figure 8 f,g) due to the harmonics generated by the MSC. This noise is small (~1.9% of rated peak current) but further investigation is required into their impact on ΔT_j before the noise can be deemed negligible.

Figure 8.h-j shows the complexity of the current throughput of the power modules in the MSC. The current varies significantly at various frequencies due to the current demanded of the generator (h), the direction of the current (i), and the switching pattern of the IGBTs (j). This large amount of complexity could not be directly derived from the present wind speed.

The turbine responds successfully to this reduction in wind speed in the MPPT region. The I_q response is dictated by the ω_t response indicating that the drive train dynamics cannot be neglected. The current noise due to harmonics is small, but further investigation is required to determine if it can be neglected. The current in the power modules is complex and cannot be directly derived from the current wind speed.

b. Wind Speed Ramp from MPPT to Rated Operating Region

Figure 9 details the turbine response to a ramp in wind speed from 11m/s to 13.5m/s; from the MPPT to rated operating region. The turbine rated wind speed (u_{rat}) is 12.7m/s. After the disturbance the turbine successfully reaches steady state at the rated turbine power ($P_{t,rat}$) (b) and $\omega_{t,rat}$ (c).

The turbine response is slower than in Section IV.a and is more complex. Figure 9.d shows that the turbine initially starts in the torque control region until $\omega_{t,rat}$ is reached, where T_{ref} remains constant and the pitch controller takes over (Figure 9.e). However due to pitch controller overshoot the ω_t drops below rated again, activating the torque control again. Therefore interaction between the controllers occurs and the current on the device has increased variation (Figure
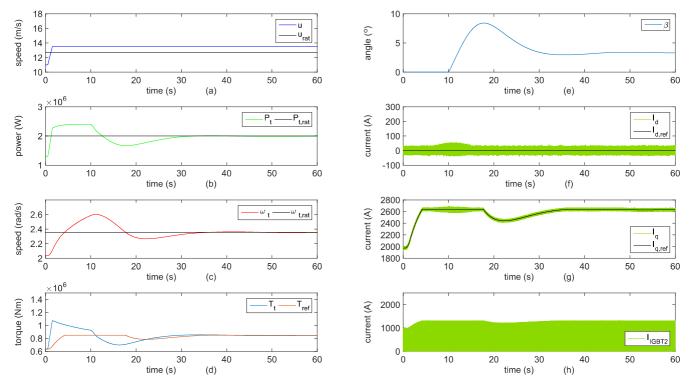

Figure 9: Turbine response to wind speed ramp from 11 to 13.5m/s: (a) wind speed, (b) turbine power, (c) turbine speed, (d) turbine torque, (e) pitch angle, (f, g) generator d,q current and (h) IGBT current.

9.h). This may increase ΔT_j, affecting device lifetime.

The interaction between controllers may be avoided by disabling the torque controller when the pitch controller is active, but the response of the turbine would be slower as ω_t would decrease even further.

Figures 9.f,g show an increase in noise in the $I_{d,q}$ currents and occurs when the ω_t is higher than rated. This noise increase is due to the increasing ω_g, causing changes in the generator voltage which must be matched by the converter output voltage Whether this impacts converter lifetime needs further investigation with thermal modelling and physical testing but it does indicate an increase in converter current loading due to the pitch controller response.

The turbine responds successfully in both MPPT and rated operating regions. The pitch controller overshoot causes interaction between the controllers and potentially increases the thermal loading on the converter power modules. The increased ω_t also increases the noise on the current signals.

c. Turbulent Wind Speed Profile

Figure 10 details the current response of one IGBT in the MSC to a turbulent wind speed input of 60s. The wind speed was simulated using the normal turbulence model (21) [24] with a mean hub wind speed (V_{hub}) of 8m/s and turbulence intensity (I_{ref}) of 0.12. The wind speeds were produced for each second and the intermediate wind speeds linearly interpolated.

$$\sigma_1 = I_{ref}(0.75V_{hub} + 5.6) \tag{20}$$

Where σ_1 is the turbulence standard deviation.

There a number of points to highlight from Figure 10:

- There are delays in the peaks in wind speed and peaks in current, but the response appears much faster than in Figure 8. This is as the turbine cannot reach its maximum operating condition as
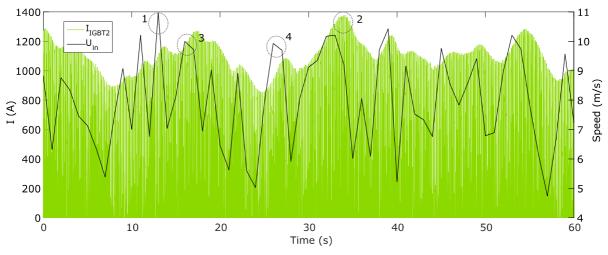
the wind speed changes too quickly. If the wind speed remained at the same wind speed for longer the currents would be higher.

- The highest wind speed |1| does not correspond to the highest current |2|. As the wind does not remain at |1|, the wind does not have the power to speed up the turbine sufficiently to reach optimum operating conditions. In contrast the lower but sustained wind speed before |2| allows the turbine get closer to the optimum operating point.
- The wind speeds |3| and |4| are similar, but give different current responses. The current at |3| is higher as the wind speed prior to this peak is higher than the wind speeds before |4|. The wind speed history is just as important as the present wind speed in determining the current throughput of the converter.

The turbulent wind speed has highlighted that the current in the converter cannot be directly derived from the present wind speed, and the dynamics of the drive train and the wind speed history must be considered.

d. Summary

The turbine responded successfully to both isolated wind speed scenarios. The turbine response is dominated by the response in ω_t which is limited by the drive train dynamics. This aspect smooths the current response of the turbine compared to if the current was derived directly from the wind speed. The current was also affected by noise from the MSC which was exasperated by the rise in ω_t above rated. The pitch controller overshoot causes interaction between the controllers and potentially increases the thermal loading on the converter power modules due to greater variation in current. The turbulent wind speed has highlighted the need to also consider the wind speed history in deriving the current throughput. Therefore the power module current throughput is complex and cannot be directly derived from the current wind speed but requires a drive train model.

As the ΔT_j is closely related to the converter current

Figure 10: IGBT current response to turbulent wind speed.

[25], the characterisation of thermal loading on the devices in the converter requires this complex drive train modelling. However in these simulations it has been assumed that all aspects of the current profile, including noise due to harmonics, are important for thermal loading and damage accumulation on the converter power modules. This assumption requires further investigation through the thermal modelling of the power modules in question and experimental validation as mentioned in Section II. This investigation can determine if aspects of the drive train can be simplified for long-term simulation.

V.   Conclusion

Maintaining high reliability of offshore wind turbines is essential for reducing the LCoE of offshore wind. It has been established that FRC reliability is critical for PMSG turbines and requires investigation into the reasons for their high failure rate. To address this, an experimental rig is being designed which will apply the power converter under turbine operating conditions.

Prior to this experimental work the potentially harmful operating conditions need to be characterised. The experimental rig also needs parameterisation. This paper outlines a computer simulation of a turbine drive train that is used to meet these objectives.

The drive train model consists of a 2MW FRC PMSG turbine with MPPT achieved using torque control and rated operation maintained using an active pitch system. with detailed models for rotor power extraction, drive train dynamics, generator, MSC, DC link and turbine control.

The drive train model was subjected to a reduction in wind speed in the MPPT operating region, a ramp up in wind speed from MPPT to rated operation, and a turbulent wind speed input. The turbine responded successfully to both isolated wind speed scenarios. The turbine response is dominated by the response in ω_t, smoothing the current. The current was also affected by noise from the MSC. Pitch controller overshoot caused interaction between the controllers, potentially increasing the thermal loading on the converter power modules. The turbulent wind speed highlighted the need to also consider wind speed history and drive train dynamics.

With this converter current response detailed simulation and analysis of the thermal loading on the power modules is possible. The turbine can now also be emulated using the AC power supply in the experimental rig to provide realistic operating conditions for the MSC power modules.

References

[1].   E. Davey and A. Nimmo. *Offshore Wind Cost Reduction, Pathways Study*. 2012 [cited 2015 07/10]; Available from: http://www.thecrownestate.co.uk/energy-and-infrastructure/offshore-wind-energy/working-with-us/strategic-workstreams/cost-reduction-study/.

[2].   W. Musial and B. Ram. *Large-Scale Offshore Wind Power in the United States: Assessment of Opportunities and Barriers*. 2010 [cited 2015 07/10]; Available from: http://www.nrel.gov/docs/fy10osti/40745.pdf.

[3].   F. Spinato, et al., *Reliability of wind turbine subassemblies.* Renewable Power Generation, IET, 2009. 3(4): p. 387-401.

[4].   J. Carroll, A. McDonald, and D. McMillan, *Failure rate, repair time and unscheduled O&M cost analysis of offshore wind turbines.* Wind Energy, 2015.

[5].   J. Carroll, A. McDonald, and D. McMillan, *Reliability Comparison of Wind Turbines With DFIG and PMG Drive Trains.* IEEE Transactions on Energy Conversion, 2015. 30(2): p. 663.

[6].   H. Wang, K. Ma, and F. Blaabjerg. *Design for reliability of power electronic systems*. in *IECON 2012 - 38th Annual Conference of IEEE Industrial Electronics*. 2012.

[7].   G. Van Bussel and M. Zaaijer. *Reliability, availability and maintenance aspects of large-scale offshore wind farms, a concepts study*. in *Proceedings of MAREC*. 2001.

[8].   S.S. Gjerde and T.M. Undeland. *The best suitable multilevel converters for offshore wind power generators without transformers*. in *International Power Electronics Conference (IPEC)*. 2010.

[9].   A. Sannino, H. Breder, and E.K. Nielsen. *Reliability of Collection Grids for Large Offshore Wind Parks*. in *International Conference on Probabilistic Methods Applied to Power Systems*. 2006.

[10].   K. Ma, et al., *Thermal loading and lifetime estimation for power device considering mission profiles in wind power converter.* IEEE Transactions on Power Electronics, 2015. 30(2): p. 590-602.

[11].   T. Burton, et al., *Wind energy handbook*. 2001: John Wiley & Sons.

[12].   O. Anaya-Lara, et al., *Wind energy generation: modelling and control*. 2011: John Wiley & Sons.

[13].   S.S. Rao and F.F. Yap, *Mechanical vibrations*. Vol. 4. 1995: Addison-Wesley Reading.

[14].   SEMIKRON. *SKS B1 090 GD 69/11 - MA PB Datasheet*. 2013 [cited 2015 13/10]; Available from: http://www.semikron.com/dl/service-support/downloads/download/semikron-datasheet-sks-b1-090-gd-69-11-ma-pb-08800136.

[15].   SEMIKRON. *SKiiP 1513 GB172-3DW V3 Datasheet*. 2014 [cited 2015 13/10]; Available from: http://www.semikron.com/dl/service-support/downloads/download/semikron-datasheet-skiip-1513-gb172-3dw-v3-20451120.

[16].   MathWorks. *Universal Bridge*. 2015 [cited 2015 07/10]; Available from: http://uk.mathworks.com/help/physmod/sps/powersys/ref/universalbridge.html.

[17].   SEMIKRON. *Optimised Converter for Solar and Wind*. 2014 [cited 2015/ 14/09]; Available from: http://www.semikron.com/dl/service-

support/downloads/download/semikron-flyer-semistackre-2014-04-08.

[18]. SEMIKRON. *Semistack RE Datasheets.* 2015 [cited 2015 14/09]; Available from: http://www.semikron.com/products/product-classes/stacks.html#presets/product-line=semistack-re/.

[19]. M. Chinchilla, S. Arnaltes, and J.C. Burgos, *Control of permanent-magnet generators applied to variable-speed wind-energy systems connected to the grid.* IEEE Transactions on Energy Conversion, 2006. 21(1): p. 130-135.

[20]. J. Zhang, et al. *Pitch angle control for variable speed wind turbines.* in *Third International Conference on Electric Utility Deregulation and Restructuring and Power Technologies.* 2008.

[21]. F.D. Bianchi, H. De Battista, and R.J. Mantz, *Wind turbine control systems: principles, modelling and gain scheduling design.* 2006: Springer Science & Business Media.

[22]. Mathworks. *Universal Bridge.* 2015 [cited 2015 14/09]; Available from: http://uk.mathworks.com/help/physmod/sps/powersys/ref/universalbridge.html.

[23]. B. Wu, et al., *Power conversion and control of wind energy systems.* 2011: John Wiley & Sons.

[24]. I.E. C, *Wind turbines-Part 1: Design requirements,* 2005: IEC 61400-1:2005(E).

[25]. P. Wyllie, *Electrothermal Modelling for Doubly Fed Induction Generator Converter Reliability in Wind Power,* 2014, Durham University Thesis.

[26]. J. Slootweg, H. Polinder, and W. Kling. *Dynamic modelling of a wind turbine with doubly fed induction generator.* in *Power Engineering Society Summer Meeting.* 2001.

[27]. B. Wu, Y. Lang, and S. Kouro, *Power conversion and control of wind energy systems,* 2011, John Wiley and Sons, Inc., NJ, USA.

[28]. V. Akhmatov, *Analysis of dynamic behaviour of electric power systems with large amount of wind power,* 2003, Electric Power Engineering, Ørsted-DTU, Technical University of Denmark Thesis.

[29]. J.-B. Sim, et al., *Ride-through of PMSG wind power system under the distorted and unbalanced grid voltage dips.* Journal of Electrical Engineering & Technology, 2012. 7(6): p. 898-904.

[30]. F.M. Gonzalez-Longatt, P. Wall, and V. Terzija. *A simplified model for dynamic behavior of permanent magnet synchronous generator for direct drive wind turbines.* in *2011 IEEE Trondheim PowerTech.* 2011.

Appendix A

Parameter	Value	Reference
A_t	0.22	[26]
B_t	116	[26]
C_t	0.4	[26]
D_t	0	[26]
E_t	0	[26]
F_t	5	[26]
G_t	12.5	[26]
H_t	0.08	[26]
K_t	0.035	[26]
$P_{t,rat}$	2.0MW	[27]
$\omega_{t,rat}$	22.5rpm	[27]
λ_{opt}	6.3	-
$C_{p,max}$	0.438	-
$C_{p,betz}$	0.593	[12]
u_{rat}	12.7m/s	-
r	34m	-
ρ	1.225kg/m^3	[12]
J_t	2.92x10^6 kg/m^2	[28]
J_g	200kg/m^2	[29]
K	4.0x10^7 Nm/rad	[28]
C_d	6.72x10^6 Nms/rad	-
R_s	8.21x10^{-4} Ω	[23]
L_d	1.5731H	[23]
p	52	[23]
φ	8.24Vs (peak)	[23]
V_f	0.95	[15]
V_{fd}	1.9V	[15]
T_f	0	-
T_t	0	-
R_{on}	1.2mΩ	[15]
V_{dc}	1150V	-
R_{snub}	1x10^5 Ω	[16]
C_{snub}	inf F	[16]
$R_{c/r}$	200	-
β_{max}	45°	SG
β_{min}	0°	SG
$\beta_{rate,max}$	8°/s	SG
$\beta_{rate,min}$	-8°/s	SG
τ	0.5s	[30]
P_p	3.357	-
I_p	0.012	-
P_{id}	-0.148	-
I_{id}	-5.377	-
P_{iq}	-0.155	-
I_{iq}	-2.689	-

Table A: Drive train parameters.

V_f is the IGBT forward voltage (V), V_{fd} is the diode forward voltage (V), $T_{f,t}$ is the IGBT fall time and tail time respectively (s), R_{on} is the IGBT on state slope resistance (Ω) is. R_{snub} is the snubber resistance (Ω), C_{snub} is the snubber capacitance (F), $P_{p,id,iq}$ are the proportional gains for the pitch, I_d and I_q controllers respectively, and $I_{p,id,iq}$ are the integral gains for the pitch, I_d and I_q controllers respectively.

Those labelled 'SG' are from the exemplar wind turbine from the Supergen wind hub: http://www.supergen-wind.org.uk/